OI 630.0 nm and N_2 1PG emissions in pulsating aurora events observed by an optical spectrograph at Tromsø, Norway

T. T. Tsuda[1], C. Li[1], S. Hamada[1], K. Hosokawa[1], S.-i. Oyama[2,3,4], S. Nozawa[2], T. Kawabata[2], A. Mizuno[2], J. Kurihara[5], T. Nishiyama[3,6], and M. J. Kosch[7,8,9]

[1]Department of Computer and Network Engineering, University of Electro-Communications (UEC), Chofu, Japan
[2]Institute for Space-Earth Environmental Research (ISEE), Nagoya University, Nagoya, Japan
[3]National Institute of Polar Research (NIPR), Tachikawa, Japan
[4]Space Physics and Astronomy Research Unit, University of Oulu, Oulu, Finland
[5]Department of Earth and Planetary Sciences, Hokkaido University, Sapporo, Japan
[6]Department of Polar Science, The Graduate University for Advanced Studies, SOKENDAI, Tachikawa, Japan
[7]South African National Space Agency (SANSA), Hermanus, South Africa
[8]Department of Physics, Lancaster University, Lancaster, UK
[9]Department of Physics and Astronomy, University of the Western Cape, Bellville, South Africa

Key Points:

- Pulsating aurora events were observed by an optical spectrograph.
- ON and OFF spectra showed OI 630.0 nm as well as N_2 1PG emissions.
- Dominant pulsations around 630.0 nm were due to N_2 1PG (10,7) emissions.

Corresponding author: T. T. Tsuda, takuo.tsuda@uec.ac.jp

Abstract

We performed observations of pulsating aurora (PsA) with an optical spectrograph at Tromsø, Norway, during wintertime in 2016–2017. The data analysis of multiple PsA events revealed the PsA spectra for the first time. As the results, the OI 630.0 nm emissions as well as the N_2 1PG emissions were found in the both spectra during brighter (ON) and darker (OFF) phases in the PsA events. The spectra of pulsations were derived as difference spectra between the ON and OFF spectra. From the obtained spectra of pulsations, it is found that dominant pulsations at 630.0 nm were coming from the N_2 1PG (10,7) band, and there were less or minor contributions of the OI 630.0 nm to pulsations at 630.0 nm.

1 Introduction

Pulsating aurora (PsA) is a diffuse-type aurora, and is characterized by a repetition of brighter (ON) and darker (OFF) emissions with periods of a few to a few tens of seconds (cf. Oguti et al., 1981; Yamamoto, 1988; Hosokawa & Ogawa, 2015; Miyoshi, Oyama, et al., 2015; Miyoshi, Saito, et al., 2015, and references therein). One of interesting topics related with PsA would be that there are previous observations indicating OI 630.0 nm pulsations (e.g., Eather, 1969; Liang et al., 2016; Nozawa et al., 2018), while the OI 630.0 nm emission, $O(^1D)$, has a long radiative lifetime, 110 s (cf. Jones, 1971, 1974), compared with the PsA periods.

Eather (1969) reported pulsations with ON-OFF periods of 2–20 s in the 630.0 nm channel from PsA observations by a tilting-filter photometer (Eather & Reasoner, 1969), and its periods were significantly faster than the $O(^1D)$ lifetime (110 s). Liang et al. (2016) conducted PsA observations with 3 s cadence by a high sensitive imager equipped with a bandpass-filter for 630.0 nm, and found PsA-related modulations in the 630.0 nm emission intensity. PsA observations with 400 Hz data sampling rate using a multi-wavelength photometer (Nozawa et al., 2018) showed pulsations in the 630.0 nm channel, in addition to pulsations in the 427.8 nm (N_2^+ 1NG (0,1)), the 557.7 nm (OI 557.7 nm) and so on. It is noted that the lifetimes of N_2^+ 1NG and OI 557.7 nm are 70 ns (i.e., prompt emission) and 0.7 s, respectively (cf. Jones, 1971, 1974).

As an explanation for such 630.0 nm pulsations, Eather (1969) suggested a possibility of more rapid OI 630.0 nm emissions caused by the quenching effect. The quenching effect is suppression of slower OI 630.0 nm emissions by collisions with ambient atmospheric particles, and as the result only faster OI 630.0 nm emissions can survive. During this process, most of $O(^1D)$ can be lost by the collisions (not by the radiative emissions). Hence, the OI 630.0 nm emission intensity can be significantly reduced. The collisions become more significant in higher atmospheric densities at lower heights. For example, the observed OI 630.0 nm emission lifetimes are 100 s at 350 km height and 20 s at 200 km height (cf. Kalogerakis et al., 2009). Considering the quenching effect, Liang et al. (2016) successfully produced OI 630.0 nm pulsations with 6–15 s periods around 150–160 km heights by a time-dependent emission model.

The processes can be summarized as the following equations (cf. Gustavsson et al., 2001; Kalogerakis et al., 2009). As the excitation process, the energetic electrons (e^*), which are precipitating from the magnetosphere, can produce $O(^1D)$ (see Equation 1). Then, $O(^1D)$ can be lost due to the quenching effect by the ambient particles, N_2, O_2, and O (see Equations 2–4), or due to the radiative emissions (see Equations 5–7). It is noted that the transition probabilities in the radiative emission processes are $A_2 = 0.0071\ s^{-1}$ for 630.0 nm, $A_1 = 0.0022\ s^{-1}$ for 636.4 nm, and $A_0 = 1.1\times10^{-6}\ s^{-1}$ for 639.2 nm, providing a total radiative probability, $A = A_0 + A_1 + A_2$, which corresponds to an effective radiative lifetime of $\sim$107 s (cf. Gustavsson et al., 2001).

$$\mathrm{O} + \mathrm{e}^* \rightarrow \mathrm{O}(^1\mathrm{D}) + \mathrm{e}^* \tag{1}$$

$$\mathrm{O}(^1\mathrm{D}) + \mathrm{N}_2 \rightarrow \mathrm{O}(^3\mathrm{P}) + \mathrm{N}_2 \tag{2}$$

$$\mathrm{O}(^1\mathrm{D}) + \mathrm{O}_2 \rightarrow \mathrm{O}(^3\mathrm{P}) + \mathrm{O}_2 \tag{3}$$

$$\mathrm{O}(^1\mathrm{D}) + \mathrm{O} \rightarrow \mathrm{O}(^3\mathrm{P}) + \mathrm{O} \tag{4}$$

$$\mathrm{O}(^1\mathrm{D}) \rightarrow \mathrm{O}(^3\mathrm{P}_2) + h\nu\ (630.0\ \mathrm{nm}) \tag{5}$$

$$\mathrm{O}(^1\mathrm{D}) \rightarrow \mathrm{O}(^3\mathrm{P}_1) + h\nu\ (636.4\ \mathrm{nm}) \tag{6}$$

$$\mathrm{O}(^1\mathrm{D}) \rightarrow \mathrm{O}(^3\mathrm{P}_0) + h\nu\ (639.2\ \mathrm{nm}) \tag{7}$$

In the PsA event by Nozawa et al. (2018), it was found that there was a time delay between emissions in the 427.8 nm (70 ns lifetime) and 557.7 nm (0.7 s lifetime), but there was no time delay between emissions in the 427.8 nm and 630.0 nm (110 s lifetime or shorter at lower heights). The time delay in the 557.7 nm would be explained by the longer lifetime of OI 557.7 nm, compared with that of 427.8 nm. There might be the quenching effect on OI 557.7 nm, which could make its emission lifetime shorter (cf. Scourfield et al., 1971; Brekke & Henriksen, 1972; Kawamura et al., 2020). However, their results indicate that the time delay can survive in the case of 557.7 nm. Although the lifetime of OI 630.0 nm would be longer than that of OI 557.7 nm (if there is a certain amount of the quenching effect), no time delay was observed in the case of 630.0 nm. Thus, it may be difficult to explain such faster 630.0 nm emissions (compared with the 557.7 nm) only by the quenching effect.

Another explanation may be that the 630.0 nm emission can include contamination from the N_2 1PG, whose lifetime is 6 μs (i.e., prompt emission) (Jones, 1971, 1974). As shown by Jones (1971, 1974), the N_2 1PG (10,7) 632.3 nm band can be extending over 630.0 nm, while its emission intensity would be normally much smaller than the OI 630.0 nm emission. On the other hand, for the OI 630.0 nm pulsations, its emission intensity should be largely reduced by the quenching effect.

Here, an important question is whether the quenched OI 630.0 nm emission is larger or smaller than the contamination by the N_2 1PG (10,7) band. To clarify this point, in the present work we have analyzed PsA events using observational data obtained by a compact optical spectrograph (cf. Oyama et al., 2018). This kind of spectral observation in PsA emission has not been performed before. Our work reveals PsA spectra for the first time, and its spectral shapes can provide information on separation of the line-shaped OI 630.0 nm emission and the band-shaped N_2 1PG (10,7) emission.

2 Observations

Using the optical spectrograph, we made aurora observations during wintertime in 2016–2017, at the European incoherent scatter (EISCAT) radar Tromsø site, Norway (69.6°N, 19.2°E). The spectrograph mainly consists of a compact imaging spectrometer (Princeton Instruments, IsoPlane-160) and an air-cooled chargecoupled device (CCD) imager (Princeton Instruments, PIXIS256E). We note that it has originally the imaging capability for spatial and spectral information with the two-dimensional CCD imager (1024×256 pixels), but we set 1×256 binning along the spatial direction to enhance signal-to-noise ratio (SNR) and to reduce data amount. Thus, the obtained data with the resulting 1024 pixels have only spectral information (not including spatial information), which covers a wavelength range of ∼400 nm in the visible to near infrared region (480–880 nm) with an interval of ∼0.4 nm and a resolution of ∼1.6 nm. An achromatic lens (Tokiwa Optical Corporation, TS-0372A5) is used as a simple receiving optics, with a high-reflection (HR) coated mirror (Thorlabs, BB2-E02) for steering optical path. The field-of-view (FOV) is $0.03° \times 2°$, and it is pointed at elevation of 78° and azimuth of 180° which is near the local geomagnetic field-aligned direction. The exposure time is 0.7 s, and the data sampling interval is 1 s. This data sampling rate (1 Hz) would be fast enough for observations of ON-OFF pulsations (i.e., main pulsations) during PsA with periods of a few to a few tens of seconds. On the other hand, the observations cannot detect a few Hz internal modulations (e.g., Nishiyama et al., 2014) embedded in main pulsations because of the limitation of the time resolution. These observation parameters are briefly summarized in Table 1, and an overview of the instrument is shown in Figure 1.

3 Results

At first, we report on a PsA event from 03:00 to 04:00 UT on 6 March 2017. Figure 2 shows time-wavelength variation in the emission intensity observed by the spectrograph during the 60 min. As mentioned in the previous section (see Table 1), the time and wavelength intervals are 1 s and ∼0.4 nm, respectively. We can see many vertical stripes continuously during the 60 min, and each stripe corresponds to each pulsation (i.e., ON and OFF). This kind of long-lasting PsA event is useful to improve data quality (i.e., SNR) by data averages. It should be noted that an increase in the emission intensity around <550 nm at 03:40–04:00 UT was due to the beginning of sunlight (i.e., the dawn).

A time-averaged PsA spectrum for the 60-min from 03:00–04:00 UT is shown in Figure 3a. The averaged spectrum includes data during the both ON and OFF phases in the PsA event. The most intense auroral emission was the line-shaped OI

557.7 nm, and then we can find more auroral emissions such as the OI 630.0 nm, N_2 1PG, and so on. It should be noted that the widths of line emissions would be mainly due to the limitation of the wavelength resolution (∼1.6 nm). As shown in Figure 3b, the line-shaped OI 630.0 nm emission was clearly found. As for the N_2 1PG band system, three bands were clearly seen from 655 to 680 nm, which correspond to the N_2 1PG (4,1) 678.9 nm, N_2 1PG (5,2) 670.5 nm, and N_2 1PG (6,3) 662.4 nm bands. The N_2 1PG (7,4) 654.5 nm and N_2 1PG (8,5) 646.9 nm bands were also found as two peaks around 640–655 nm. Around 635–640 nm, it seems that there was the N_2 1PG (9,6) 639.5 nm band and it was overlapping with the line-shaped OI 636.4 nm. Also the N_2 1PG (10,7) 632.3 nm band seemed to be overlapping with the line-shaped OI 630.0 nm around 625–635 nm, but its emission intensity was much smaller than that of the OI 630.0 nm.

To see the pulsations (i.e., ON-OFF variation) of the PsA event in more detail, we have made the wavelength-averaged data in two wavelength ranges for each 1-s sampling data. A wavelength range covers 630.0 nm emission, and the other covers three N_2 1PG bands (see green curves in Figure 3). The range for 630.0 nm emission can include both the OI 630.0 nm and the N_2 1PG (10,7). The range for N_2 1PG emission include the N_2 1PG (4,1) 678.9 nm, N_2 1PG (5,2) 670.5 nm, and N_2 1PG (6,3) 662.4 nm bands, and it would be pure N_2 1PG emissions (i.e., no contamination from other atoms and molecules). Figure 4 shows time variations in the wavelength-averaged N_2 1PG and 630.0 nm intensity data during a part of the PsA event. In the averaged N_2 1PG emission, clear ON-OFF variation can be seen. Similar ON-OFF variation can be seen also in the averaged 630.0 nm emission, while its data quality was not so high compared with that of the averaged N_2 1PG data because of the numbers of data points used for the averages. The period of the observed pulsations was roughly 10 s. For the following data analysis, we selected periods of relatively stable pulsations and determined ON and OFF phases based on the time series in the N_2 1PG emission by manual inspection. The ON and OFF phases were marked by red and blue, respectively (see Figure 4).

According to the determined ON and OFF phases (see Figure 4), we made the averaged ON and OFF spectra for 03:27–03:40 UT separately. The number of spectra at the ON phases was 360, and that at the OFF phases was 194 (see Table 2). These obtained ON and OFF spectra are shown in Figure 5. For the both ON and

OFF spectra, the most intense emissions were the OI 577.7 nm, and more auroral emissions can be found, such as the OI 630.0 nm, the N_2 1PG, and so on. In much similar way as the 60-min integrated spectrum (including the both ON and OFF time), there were the line shape of the OI 630.0 nm and also the band structure of N_2 1PG in the both ON and OFF spectra.

Figure 6 shows a difference spectrum between the ON and OFF spectra, which corresponds to an emission spectrum contributing to the pulsations. Here, the background level would be well subtracted during the difference calculation. Then, as for the unit of emission intensity, we converted counts to R nm^{-1} (Rayleigh nm^{-1}) with the sensitivity calibration data, which was obtained by using the integrated sphere light source at National Institute of Polar Research (NIPR), Tachikawa, Tokyo, Japan. In the difference spectrum, there were clear seven peaks from 625 to 680 nm. These would correspond to the seven N_2 1PG bands, which are the N_2 1PG (4,1) 678.9 nm, N_2 1PG (5,2) 670.5 nm, N_2 1PG (6,3) 662.4 nm, N_2 1PG (7,4) 654.5 nm, N_2 1PG (8,5) 646.9 nm, N_2 1PG (9,6) 639.5 nm, and N_2 1PG (10,7) 632.3 nm. Widths of these bands were roughly 5–10 nm. On the other hand, there was no clear signature in the line-shaped emissions due to the OI 630.0 nm and OI 636.4 nm. These results would indicate that the observed pulsations from 625 to 680 nm were produced mainly due to the N_2 1PG bands (not due to the OI 630.0 nm and/or OI 636.4 nm). The emission intensity at 630.0 nm was $\sim$20 R nm^{-1}, which would be mainly due to the N_2 1PG (10,7) 632.3 nm band.

We have done same data analysis for eight PsA events (including the first event), and the event list is summarized in Table 2. In all the events, the ON and OFF spectra showed clear signatures in the OI 630.0 nm as well as the N_2 1PG (not shown here). Concerning to the difference spectra, the seven N_2 1PG bands were clearly found in all the events, as shown in Figure 7. On the other hand, there was no significant signature in the line-shaped OI 630.0 nm and OI 636.4 nm in all the events (see Figure 7).

4 Discussion and Conclusions

The present work revealed the PsA spectra from the multi-event data analysis by using the spectrograph observations. Here, based on the obtained PsA spectra, we discuss some indications of PsA-related energetic electrons and/or chorus waves, while it does not include observational data on energetic electrons and/or chorus waves. Comparative studies on PsA spectra along with such observational data would be important for more evidence-based investigation in the future, but it is beyond the scope of the present work.

It is considered that PsA can be related with high-energy electrons (>3 keV) and low-energy electrons (up to 1 keV), and the both high- and low-energy electrons can be generated by lower-band chorus waves and upper-band chorus waves, respectively (cf. Miyoshi, Saito, et al., 2015). Then, the N_2 1PG emission can be generally induced by the high-energy electrons, and the OI 630.0 nm emission can be generally induced by the low-energy electrons (cf. Ono, 1993; Ono & Morishima, 1994; Semeter et al., 2001; Lanchester et al., 2009). As shown in the previous section, the observed ON spectra showed that there were the OI 630.0 nm and N_2 1PG bands in all the events. The same features were found in the OFF spectra. These results can be an indication that there would be both the high-energy and low-energy electrons related with the PsA events. Such PsA-related high-energy and low-energy electrons would induce ionization in both E and F regions, as reported from incoherent scatter radar observations (Oyama et al., 2014).

In the obtained pulsation spectra (i.e., the difference spectra), we found that there were significant pulsations due to the N_2 1PG bands in all the events. This result is not inconsistent with periodic precipitation in the high-energy electrons induced by the periodic lower band chorus bursts, suggested by Miyoshi, Saito, et al. (2015). It was reported that differential electron energy spectra between ON and OFF in PsA events were prominent around 5–40 keV from rocket observations of precipitating electrons (Sandahl et al., 1980). Our observed pulsation spectra would be optical spectra corresponding to such differential electron energy spectra. Concerning to the OI 630.0 nm, no clear pulsations were found in all the events. Thus, the N_2 1PG (10,7) 632.3 nm pulsations were major contributors for the 630.0 nm pulsations (see Figure 7). Hence, the PsA-related rapid variation in the 630 nm emission (faster than the OI 557.7 nm emission) reported by Nozawa et al. (2018) can be (at least partly) explained by the contamination of the N_2 1PG (10,7) 632.3 nm emission (6 μs lifetime).

Several reasons can be considered for the lack of clear OI 630.0 nm pulsations. First, precipitation of low-energy electrons may be relatively stable (or not periodic) due to relatively stable upper-band chorus waves (Miyoshi, Saito, et al., 2015). Second, the loss of emission intensity may be quite large due to strong quenching effect at lower heights (Eather, 1969; Liang et al., 2016). Third, because of weak quenching effect at higher heights, the OI 630.0 nm emission lifetime may be quite long compared with the periods of pulsations. The mixture of first and second reasons would be possible, and the mixture of first and third reasons would be also possible. As another reason, there might be very faint OI 630.0 nm pulsations less than the detection limits of the spectrograph. To confirm it, more sensitive observations are needed in the future.

Here, we would recognize an importance of careful observation from the fact that the dominant pulsations at 630.0 nm was mainly due to the band-shaped N_2 1PG (10,7) 632.3 nm (not the line-shaped OI 630 nm). Because the N_2 1PG (10,7) 632.3 nm band is overlapping over the OI 630.0 nm, in principle optical observations equipped with conventional bandpass filters cannot separate these two emissions. The OI 630.0 nm emission may be normally large enough for neglecting N_2 1PG (10,7) 632.3 nm emission, but it may not be the case for faint variations such as the pulsations during PsA. This means that it would be difficult to use the OI 630.0 nm as an indicator for low-energy electrons in such conditions. To solve this problem, spectral observations such as our observations can provide useful information on shapes of emission spectra, which would allow us consider these two different emissions separately.

As a final point, we have a brief consideration on alternatives to the OI 630 nm as an indicator for low-energy electrons for PsA research. For example, the OI 777.4 nm, OI 844.6 nm, and OII (O^+) 732.5 nm would be candidates (cf. Ono, 1993; Ono & Morishima, 1994; Semeter et al., 2001; Lanchester et al., 2009). Figure 8 shows the pulsation spectra from 480 to 880 nm in all the events, which are same data as Figure 7. It is found that there was no significant emission in the OII 732.5 nm. In addition, it seems that the N_2 1PG (5,3) 738.7 nm band emissions were extending over 732.5 nm. Thus, it would be difficult to use the OII 732.5 nm. On the other hand, there might be significant emissions in the OI 777.4 nm. However, a separation from the N_2 1PG (2,0) 775.4 nm would be quite difficult in the case of the current wavelength resolution (∼1.6 nm) (cf. Oyama et al., 2018). It may be possible to make a separation between the OI 777.4 nm and the N_2 1PG (2,0) if we perform observations with much higher wavelength resolution, because the N_2 1PG (2,0) band is basically extending from 775.4 nm to shorter wavelength. As for the OI 844.6 nm, we found clear line-shaped emissions due to the OI 844.6 nm. It seems that the OI 844.6 nm were relatively isolated, and there were relatively less contamination from other emissions. Thus, the OI 844.6 nm would be a most probable candidate for investigating PsA-related low-energy electrons. A combination of N_2 1PG (5,2) 670.5 nm and OI 844.6 nm was used in some case studies (Ono & Morishima, 1994; Nishiyama et al., 2016). As a next step, we should work on more quantitative investigation in the energy of PsA-related precipitating electrons, for example using a combination of the OI 844.6 nm and the N_2 1PG together with electron density data from the colocated EISCAT radars, but it is beyond the scope of the present work.

Acknowledgments

This work was supported in part by MEXT/JSPS KAKENHI grants, JP15H05747, JP15H05815, JP16H01171, JP16H06021, JP16H06286, JP17H02968, JP19H01956, JP20K20940, and JPJSBP120194814, by the Sumitomo Foundation Basic Science Research grant, 150627, by Inamori Research Grants from Inamori Foundation, by Research Grants from JGC-S Scholarship Foundation, by National Institute of Polar Research (NIPR) through General Collaboration Project, 31-3, and by the joint research program of the Institute for Space-Earth Environmental Research (ISEE), Nagoya University. The spectrograph data can be available on request to T. T. Tsuda (takuo.tsuda@uec.ac.jp) or can be available directly at the website for the spectrograph (http://ttt01.cei.uec.ac.jp/sg01/). The sensitivity calibrations for the spectrograph were done by using the integrated sphere light source at National Institute of Polar Research (NIPR), Tachikawa, Tokyo, Japan. The infrastructure for the spectrograph is supplied by Tromsø Geophysical Observatory (TGO), The Arctic University of Norway (UiT). The OMNI data, shown in Supporting Information, were obtained by using Space Physics Environment Data Analysis Software (SPEDAS) (http://spedas.org/) with a plug-in software developed by Inter-university Upper atmosphere Global Observation NETwork (IUGONET) (http://www.iugonet.org/).

References

Brekke, A., & Henriksen, K. (1972). The intensity ratio I(5577)/I(4278) and the effective lifetime of O(^{1}S) atoms in pulsating aurora. *Planetary and Space Science*, *20*(1), 53–60. Retrieved from http://www.sciencedirect.com/science/article/pii/0032063372901407 doi: https://doi.org/10.1016/0032-0633(72)90140-7

Eather, R. H. (1969). Short-period auroral pulsations in λ6300 OI. *Journal of Geophysical Research (1896–1977)*, *74*(21), 4998–5004. Retrieved from https://agupubs.onlinelibrary.wiley.com/doi/abs/10.1029/JA074i021p04998 doi: 10.1029/JA074i021p04998

Eather, R. H., & Reasoner, D. L. (1969). Spectrophotometry of faint light sources with a tilting-filter photometer. *Appl. Opt.*, *8*(2), 227–242. Retrieved from http://ao.osa.org/abstract.cfm?URI=ao-8-2-227 doi: 10.1364/AO.8.000227

Gustavsson, B., Sergienko, T., Rietveld, M. T., Honary, F., Steen, A., Brändström, B. U. E., … Marple, S. (2001). First tomographic estimate of volume distribution of HF-pump enhanced airglow emission. *Journal of Geophysical Research: Space Physics*, *106*(A12), 29105–29123. Retrieved from https://agupubs.onlinelibrary.wiley.com/doi/abs/10.1029/2000JA900167 doi: 10.1029/2000JA900167

Hosokawa, K., & Ogawa, Y. (2015). Ionospheric variation during pulsating aurora. *Journal of Geophysical Research: Space Physics*, *120*(7), 5943–5957. Retrieved from https://agupubs.onlinelibrary.wiley.com/doi/abs/10.1002/2015JA021401 doi: 10.1002/2015JA021401

Jones, A. V. (1971). Auroral spectroscopy. *Space Science Reviews*, *11*(6), 776–826. Retrieved from https://doi.org/10.1007/BF00216890 doi: 10.1007/BF00216890

Jones, A. V. (1974). Aurora. In *Geophysics and astrophysics monographs* (Vol. 9). Dordrecht, Holland: D. Reidel Publishing Company. Retrieved from https://doi.org/10.1007/978-94-010-2099-2 doi: 10.1007/978-94-010-2099-2

Kalogerakis, K. S., Slanger, T. G., Kendall, E. A., Pedersen, T. R., Kosch, M. J., Gustavsson, B., & Rietveld, M. T. (2009). Remote oxygen sensing by ionospheric excitation (ROSIE). *Annales Geophysicae*, *27*(5), 2183–2189. Retrieved from https://www.ann-geophys.net/27/2183/2009/ doi: 10.5194/angeo-27-2183-2009

Kawamura, Y., Hosokawa, K., Nozawa, S., Ogawa, Y., Kawabata, T., Oyama, S.-i., ... Fujii, R. (2020). Estimation of the emission altitude of pulsating aurora using the five-wavelength photometer. *Earth, Planets and Space*, *72*(1), 96. Retrieved from https://doi.org/10.1186/s40623-020-01229-8 doi: 10.1186/s40623-020-01229-8

Lanchester, B. S., Ashrafi, M., & Ivchenko, N. (2009). Simultaneous imaging of aurora on small scale in OI (777.4 nm) and $N_2$1P to estimate energy and flux of precipitation. *Annales Geophysicae*, *27*(7), 2881–2891. Retrieved from https://www.ann-geophys.net/27/2881/2009/ doi: 10.5194/angeo-27-2881-2009

Liang, J., Donovan, E., Jackel, B., Spanswick, E., & Gillies, M. (2016). On the 630 nm red-line pulsating aurora: Red-line emission geospace observatory observations and model simulations. *Journal of Geophysical Research: Space Physics*, *121*(8), 7988–8012. Retrieved from https://agupubs.onlinelibrary.wiley.com/doi/abs/10.1002/2016JA022901 doi: 10.1002/2016JA022901

Miyoshi, Y., Oyama, S., Saito, S., Kurita, S., Fujiwara, H., Kataoka, R., ... Tsuchiya, F. (2015). Energetic electron precipitation associated with pulsating aurora: EISCAT and Van Allen Probe observations. *Journal of Geophysical Research: Space Physics*, *120*(4), 2754–2766. Retrieved from https://agupubs.onlinelibrary.wiley.com/doi/abs/10.1002/2014JA020690 doi: 10.1002/2014JA020690

Miyoshi, Y., Saito, S., Seki, K., Nishiyama, T., Kataoka, R., Asamura, K., ... Santolik, O. (2015). Relation between fine structure of energy spectra for pulsating aurora electrons and frequency spectra of whistler mode chorus waves. *Journal of Geophysical Research: Space Physics*, *120*(9), 7728–7736. Retrieved from https://agupubs.onlinelibrary.wiley.com/doi/abs/10.1002/2015JA021562 doi: 10.1002/2015JA021562

Nishiyama, T., Miyoshi, Y., Katoh, Y., Sakanoi, T., Kataoka, R., & Okano, S. (2016). Substructures with luminosity modulation and horizontal oscillation in pulsating patch: Principal component analysis application to pulsating aurora. *Journal of Geophysical Research: Space Physics*, *121*(3), 2360–

2373. Retrieved from https://agupubs.onlinelibrary.wiley.com/doi/abs/10.1002/2015JA022288 doi: 10.1002/2015JA022288

Nishiyama, T., Sakanoi, T., Miyoshi, Y., Hampton, D. L., Katoh, Y., Kataoka, R., & Okano, S. (2014). Multiscale temporal variations of pulsating auroras: On-off pulsation and a few Hz modulation. *Journal of Geophysical Research: Space Physics*, *119*(5), 3514–3527. Retrieved from https://agupubs.onlinelibrary.wiley.com/doi/abs/10.1002/2014JA019818 doi: 10.1002/2014JA019818

Nozawa, S., Kawabata, T., Hosokawa, K., Ogawa, Y., Tsuda, T. T., Mizuno, A., ... Hall, C. M. (2018). A new five-wavelength photometer operated in Tromsø (69.6 °N, 19.2 °E). *Earth, Planets and Space*, *70*(1), 193. Retrieved from https://doi.org/10.1186/s40623-018-0962-x doi: 10.1186/s40623-018-0962-x

Oguti, T., Kokubun, S., Hayashi, K., Tsuruda, K., Machida, S., Kitamura, T., ... Watanabe, T. (1981). Latitudinally propagating on–off switching aurorae and associated geomagnetic pulsations: A case study of an event of february 20, 1980. *Canadian Journal of Physics*, *59*(8), 1131–1136. Retrieved from https://doi.org/10.1139/p81-149 doi: 10.1139/p81-149

Ono, T. (1993). Derivation of energy parameters of precipitating auroral electrons by using the intensity ratios of auroral emissions. *Journal of geomagnetism and geoelectricity*, *45*(6), 455–472. doi: 10.5636/jgg.45.455

Ono, T., & Morishima, K. (1994). Energy parameters of precipitating auroral electrons obtained by using photometric observations. *Geophysical Research Letters*, *21*(4), 261–264. Retrieved from https://agupubs.onlinelibrary.wiley.com/doi/abs/10.1029/94GL00011 doi: 10.1029/94GL00011

Oyama, S.-i., Miyoshi, Y., Shiokawa, K., Kurihara, J., Tsuda, T. T., & Watkins, B. J. (2014). Height-dependent ionospheric variations in the vicinity of nightside poleward expanding aurora after substorm onset. *Journal of Geophysical Research: Space Physics*, *119*(5), 4146–4156. Retrieved from https://agupubs.onlinelibrary.wiley.com/doi/abs/10.1002/2013JA019704 doi: 10.1002/2013JA019704

Oyama, S.-i., Tsuda, T. T., Hosokawa, K., Ogawa, Y., Miyoshi, Y., Kurita, S., ... Leyser, T. (2018). Auroral molecular-emission effects on the atomic oxygen line at 777.4 nm. *Earth, Planets and Space*, *70*(1), 166. Retrieved from https://doi.org/10.1186/s40623-018-0936-z doi: 10.1186/s40623-018-0936-z

Sandahl, I., Eliasson, L., & Lundin, R. (1980). Rocket observations of precipitating electrons over a pulsating aurora. *Geophysical Research Letters*, *7*(5), 309–312. Retrieved from https://agupubs.onlinelibrary.wiley.com/doi/abs/10.1029/GL007i005p00309 doi: 10.1029/GL007i005p00309

Scourfield, M. W. J., Parsons, N. R., Dennis, L. P., & Innes, W. F. (1971). Effective lifetime of $O(^1S)$ in pulsating aurora. *Journal of Geophysical Research (1896-1977)*, *76*(16), 3692–3699. Retrieved from https://agupubs.onlinelibrary.wiley.com/doi/abs/10.1029/JA076i016p03692 doi: 10.1029/JA076i016p03692

Semeter, J., Lummerzheim, D., & Haerendel, G. (2001). Simultaneous multispectral imaging of the discrete aurora. *Journal of Atmospheric and Solar-Terrestrial Physics*, *63*(18), 1981–1992. Retrieved from http://www.sciencedirect.com/science/article/pii/S1364682601000748 doi: 10.1016/S1364-6826(01)00074-8

Yamamoto, T. (1988). On the temporal fluctuations of pulsating auroral luminosity. *Journal of Geophysical Research: Space Physics*, *93*(A2), 897–911. Retrieved from https://agupubs.onlinelibrary.wiley.com/doi/abs/10.1029/JA093iA02p00897 doi: 10.1029/JA093iA02p00897

Table 1. Parameters of the spectrograph observations.

Observation site	Tromsø (69.6°N, 19.2°E)
Observation direction	Field-aligned (El: 78°, Az: 180°)
Field-of-view	0.03°×2°
Aperture (F-number)	∼4
Wavelength range	480–880 nm
Wavelength interval	∼0.4 nm
Wavelength resolusion	∼1.6 nm
Data sampling interval	1 sec
Exposure time	0.7 sec

Table 2. List of PsA events.

Date	Time	Number of ON spectra	Number of OFF spectra
2016-10-24	00:15–00:29 UT	266	253
2016-11-02	01:06–01:12 UT	160	69
2016-11-02	02:15–02:22 UT	147	172
2016-11-03	02:00–02:07 UT	86	178
2017-01-05	02:39–02:48 UT	104	335
2017-01-05	03:04–03:24 UT	367	614
2017-03-06	02:27–02:41 UT	134	539
2017-03-06	03:27–03:40 UT	360	194

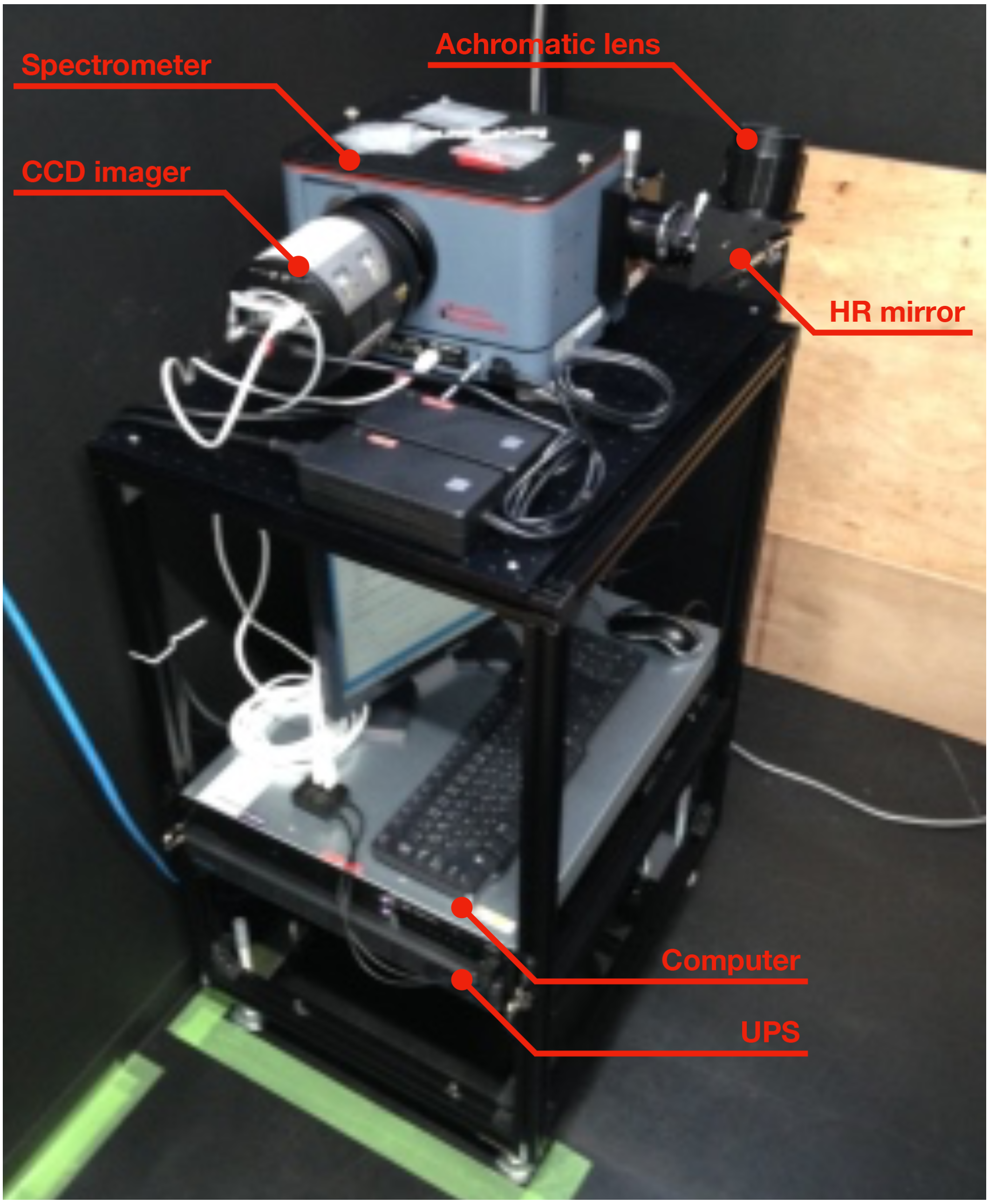

Figure 1. An overview of the spectrograph, which mainly consists of a compact imaging spectrometer (Princeton Instruments, IsoPlane-160) and an air-cooled CCD imager (Princeton Instruments, PIXIS256E). An achromatic lens (Tokiwa Optical Corporation, TS-0372A5) is used as a simple receiving optics, with a HR coated mirror (Thorlabs, BB2-E02) for steering optical path. The spectrograph is operated by a computer with an uninterruptible power supply (UPS).

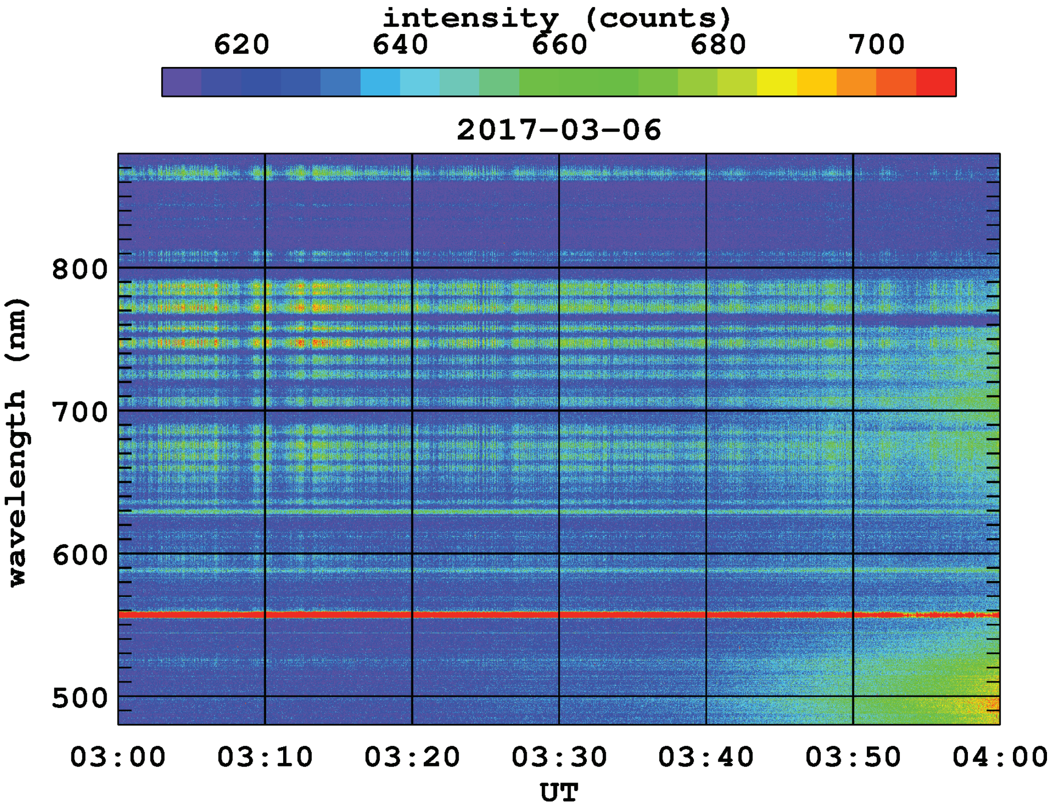

Figure 2. Time-wavelength variation in emission intensity during the PsA event at 03:00–04:00 UT on 6 March 2017 observed by the spectrograph. Vertical stripes corresponds to pulsations (i.e., ON, brighter, and OFF, darker).

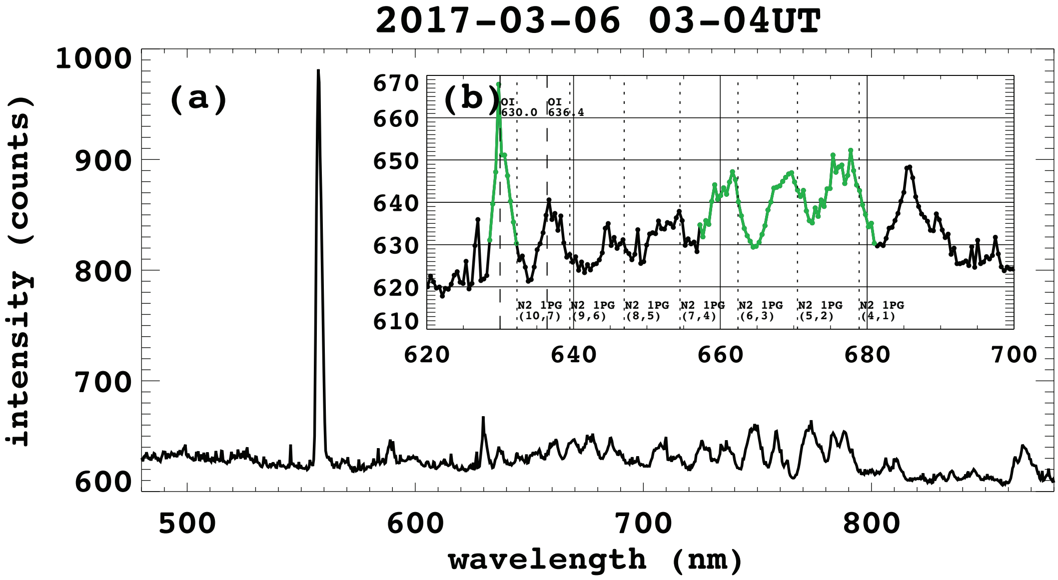

Figure 3. (a) Time-integrated PsA spectrum for 60-min (i.e., 03:00–04:00 UT) on 6 March 2017. (b) Same as (a), but for 620–700 nm. Vertical dashed lines indicate wavelengths in the OI emissions, and vertical dotted lines indicate wavelengths in the N_2 1PG emissions. Green curves indicate wavelength ranges for making wavelength-averaged intensity data for 630.0 nm (i.e., 10 data points around the OI 630.0 nm line emission) and the N_2 1PG (i.e., 60 points including three peaks in N_2 1PG bands, namely the 678.9 nm (4,1), 670.5 nm (5,2), and 662.4 nm (6,3) bands). The wavelength-averaged data are used for investigation of time variation in the PsA event.

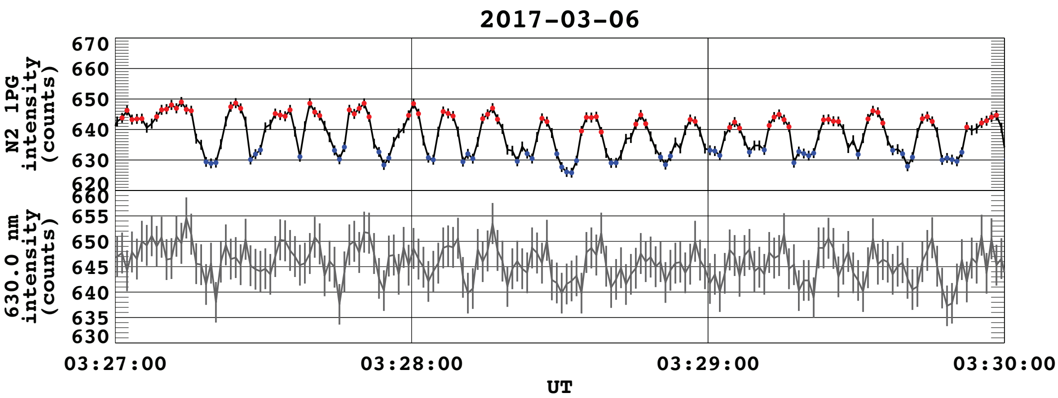

Figure 4. Time variations in the wavelength-averaged N_2 1PG (black) and 630.0 nm (gray) intensity data from 03:27 to 03:30 UT on 6 March 2017. Red and blue indicate ON and OFF of the PsA, respectively. Note that these ON and OFF were determined manually (i.e., by eyes) from the N_2 1PG variation. These ON and OFF stamps are used for making time-averaged PsA spectra for ON and OFF separately.

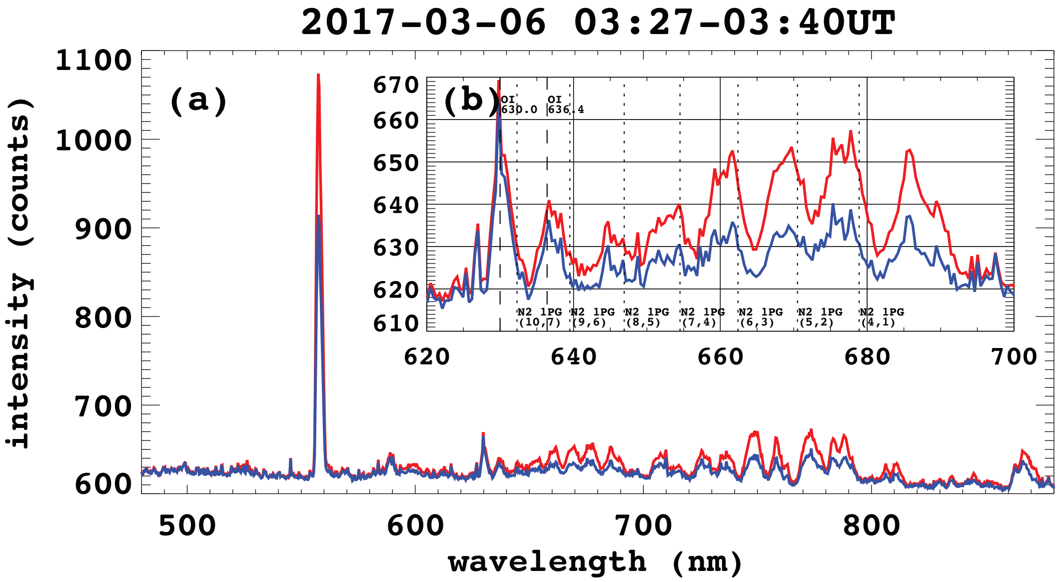

Figure 5. (a) Averaged PsA spectra for ON and OFF from 480 to 880 nm of the event at 03:27–03:40 UT on 6 March 2017. Red and blue indicate ON and OFF spectra, respectively. (b) Same as (a), but for 620–700 nm. Vertical dashed lines indicate wavelengths in the OI emissions, and vertical dotted lines indicate wavelengths in the N_2 1PG emissions. In the both ON and OFF spectra, many aurora emissions were found such as the OI 557.7 nm, the OI 630.0 nm, the N_2 1PG, and so on.

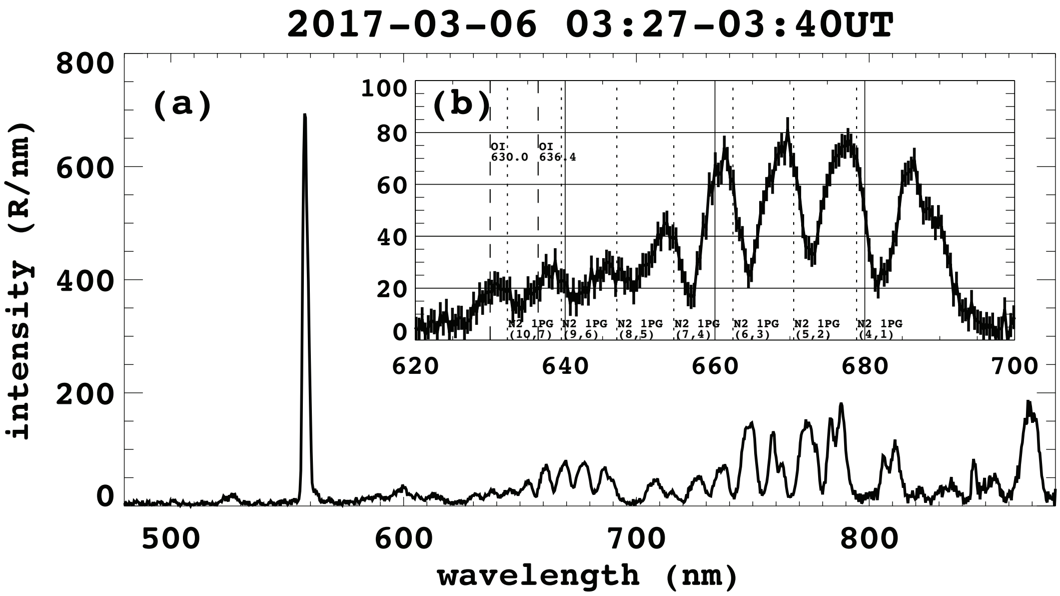

Figure 6. (a) Difference spectrum between the ON and OFF spectra from 480 to 880 nm of the event at 03:27–03:40 UT on 6 March 2017. Note that the background component is also removed by the calculation for the difference spectrum. After that, the unit of emission intensity is converted to R nm^{-1} (Rayleigh nm^{-1}). (b) Same as (a), but for 620–700 nm with error bars of 1σ. Vertical dashed lines indicate wavelengths in the OI emissions, and vertical dotted lines indicate wavelengths in the N_2 1PG emissions. Many aurora emissions were also found in the difference spectrum. The spectrum around 630.0 nm was not a line-like shape due to the OI 630.0 nm, but a band-like shape due to the N_2 1PG (10,7) band.

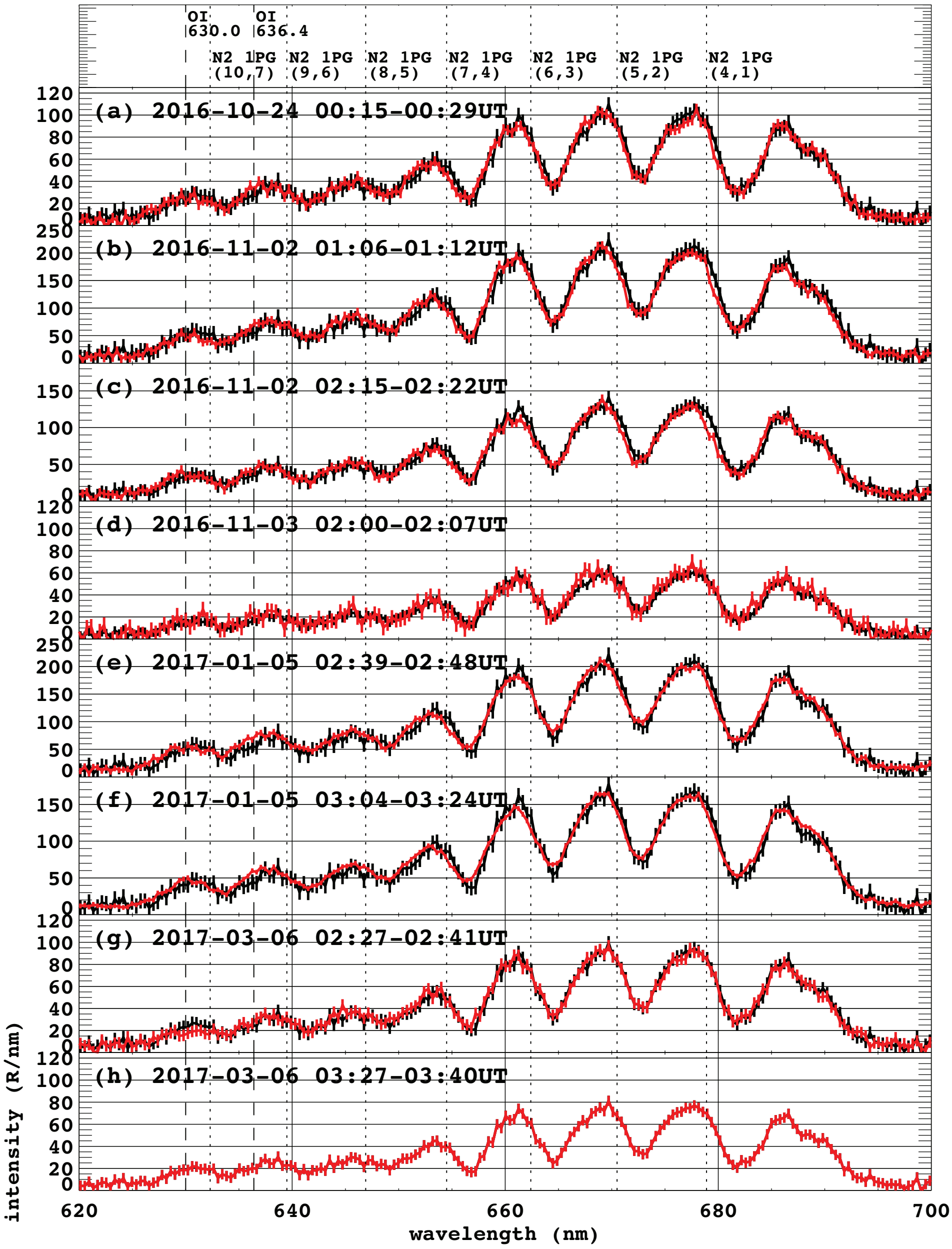

Figure 7. Difference spectra (red) in the eight PsA events during (a) 00:15–00:29 UT on 24 October 2016, (b) 01:06–01:12 UT on 2 November 2016, (c) 02:15–02:22 UT on 2 November 2016, (d) 02:00–02:07 UT on 3 November 2016, (e) 02:39–02:48 UT on 5 January 2017, (f) 03:04–03:24 UT on 5 January 2017, (g) 02:27–02:41 UT on 6 March 2017, and (h) 03:27–03:40 UT on 6 March 2017. Difference spectra (black) at 03:27–03:40 UT on 6 March 2017, which are normalized at each peak of 670.5 nm (5,2) band of each event, are also shown in each figure. It should be noted that the red is identical to the black in the figure (h). Vertical dashed lines indicate wavelengths in the OI emissions, and vertical dotted lines indicate wavelengths in the N_2 1PG emissions.

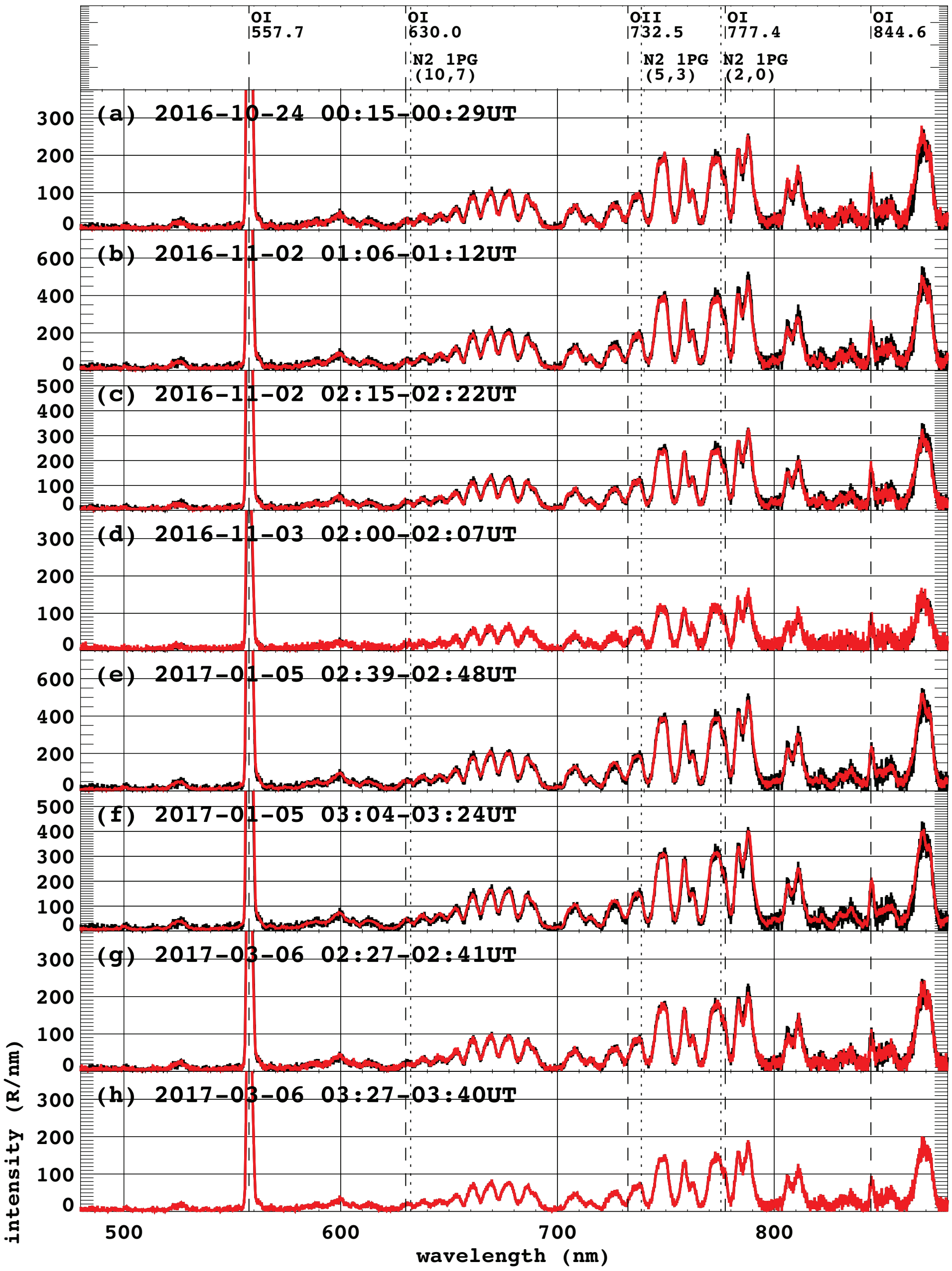

Figure 8. Same as Figure 7, but for 480–880 nm. Vertical dashed lines indicate wavelengths in the OI and OII (O^+) emissions, and vertical dotted lines indicate wavelengths in the N_2 1PG emissions.